Single and double clustering of nitrogen to Li^+

I. R. Gatland,* L. M. Colonna-Romano, and G. E. Keller
U. S. Army Ballistic Research Laboratories, Aberdeen Proving Ground, Maryland 21005
(Received 28 April 1975)

The clustering of N_2 to Li^+ has been studied experimentally using a drift tube at a gas temperature of 318 K. The gas pressure was varied between 0.5 and 1.5 Torr, and E/N (the ratio of the uniform electric field strength in the drift region to the neutral number density) was varied between 9 and 24 Td (1 Td = 10^{-17} V cm^2). Under these conditions, the major reactions are

$$Li^+ + N_2 + N_2 \underset{k_{12}}{\overset{k_{21}}{\rightleftarrows}} Li^+ \cdot N_2 + N_2 \quad \text{and} \quad Li^+ \cdot N_2 + N_2 + N_2 \underset{k_{23}}{\overset{k_{32}}{\rightleftarrows}} Li^+ \cdot 2N_2 + N_2 \ .$$

The rate coefficients and the mobilities of $Li^+ \cdot N_2$ and $Li^+ \cdot 2N_2$ were deduced by comparing measured arrival-time profiles of the ions with profiles generated by an analytical drift-tube model developed for three interreacting ion swarms. We find that the association rate coefficient k_{21} decreases from 2.0×10^{-30} cm^6/sec at $E/N = 9$ Td to 1.7×10^{-30} cm^6/sec at $E/N = 24$ Td, the collisional-dissociation rate coefficient k_{12} increases from 0.7×10^{-14} cm^3/sec at $E/N = 9$ Td to 1.6×10^{-14} cm^3/sec at $E/N = 24$ Td, and the collisional-dissociation rate coefficient k_{23} increases from 4.8×10^{-13} cm^3/sec at $E/N = 9$ Td to 6.0×10^{-13} cm^3/sec at $E/N = 24$ Td. Adequate fits could be obtained with values of k_{32} from 1.6 to 3.0 ($\times10^{-29}$) cm^6/sec; a median value of 2.2×10^{-29} cm^6/sec at all values of E/N was used to obtain the above values of the other rate coefficients. The reduced mobility (and its standard deviation) for Li^+ in N_2 was found to be 3.87 ± 0.13 cm^2/V sec; for $Li^+ \cdot N_2$ in N_2, 2.04 ± 0.12 cm^2/V sec; and for $Li^+ \cdot 2N_2$ in N_2, 1.96 ± 0.12 cm^2/V sec.

I. INTRODUCTION

We have studied the clustering of atmospheric gases to Li^+ ions using a drift tube with mass spectrometric analysis. The results of Ar clustering have been published.[1] This paper reports on the results obtained when Li^+ drifted in N_2. Preliminary results of this study were published previously.[2]

Figure 1 shows a plot of current versus ion mass as a function of the N_2 gas pressure. The source produces some sodium impurity and a small amount of neutral carbon dioxide in addition to copious quantities of Li^+ ions. The identification of the mixed cluster at mass 79 should be considered tentative. The plot is not corrected for mass discrimination in the mass sampling process, which is discussed in some detail in Ref. 1. Figure 2 shows a set of time-of-arrival profiles for the ions Li^+, $Li^+ \cdot N_2$, and $Li^+ \cdot 2N_2$. Consideration of both mass spectra and time-of-arrival profiles leads us to assume that the major reactions are

$$Li^+ + N_2 + N_2 \underset{k_{12}}{\overset{k_{21}}{\rightleftarrows}} Li^+ \cdot N_2 + N_2 \qquad (1)$$

and

$$Li^+ \cdot N_2 + N_2 + N_2 \underset{k_{23}}{\overset{k_{32}}{\rightleftarrows}} Li^+ \cdot 2N_2 + N_2, \qquad (2)$$

and that the reverse reactions must both be considered in the analysis. The four-body reaction

$$Li^+ + 3N_2 \rightarrow Li^+ \cdot 2N_2 + N_2 \qquad (3)$$

can be ruled out at these pressures, but it is possible that the reverse reaction can occur. This possibility is discussed later.

II. APPARATUS AND EXPERIMENTAL METHOD

Since the apparatus has been described previously,[1] only essential features will be described here. The drift tube is an all-metal, bakable tube which can be used with drift lengths up to 44 cm. For the work reported in this paper, the drift length for the ions was 7.48 cm, although other lengths were used for tests. The configuration of the tube is shown in Fig. 3.

The source of Li^+ ions is a platinum gauze filament coated with β-eucryptite enriched in the mass-7 isotope.[3] The source is operated at low-output current to minimize space-charge effects in the drift region.

The tube has two ion shutters. One is formed by two wire grids spaced 3.2 mm apart. The other is formed by a wire grid and the end plate of the drift tube, which are 3.2 mm apart. With the source running continuously, one of the gates is electrically biased to inhibit the drift of the ions. Then

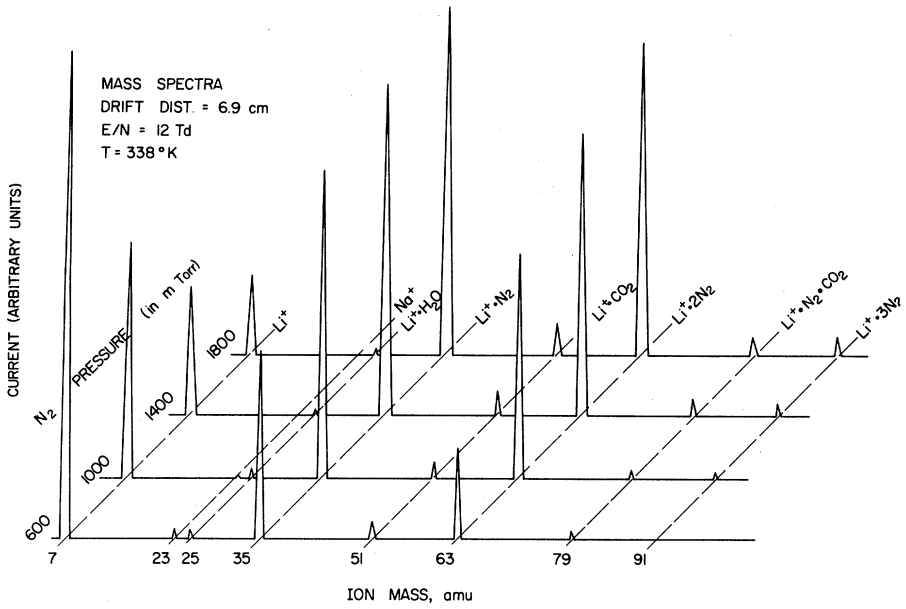

FIG. 1. Relative counting rates as a function of pressure for various ions observed in the drift tube.

this bias is momentarily reversed, which permits a small group of ions to drift down the tube from the chosen gate.

The end plate of the drift tube is electrically insulated from ground so that the current to it can be measured and, if desired, a small potential may be applied. For all the work reported here, the end plate was grounded. The exit aperture is 0.4 mm in diameter. The skimmer between the differential pumping chambers has a 4.3-mm-diam orifice in its tip, and is mounted about 3 cm from the exit aperture. The skimmer has been found to contribute to a difference in the sampling efficiency of this system for ions of different mass.[1]

The mass spectrometer is a monopole rf spectrometer modified to operate with either positive or negative ions created at ground potential. The spectrometer has better-than-unit resolution to

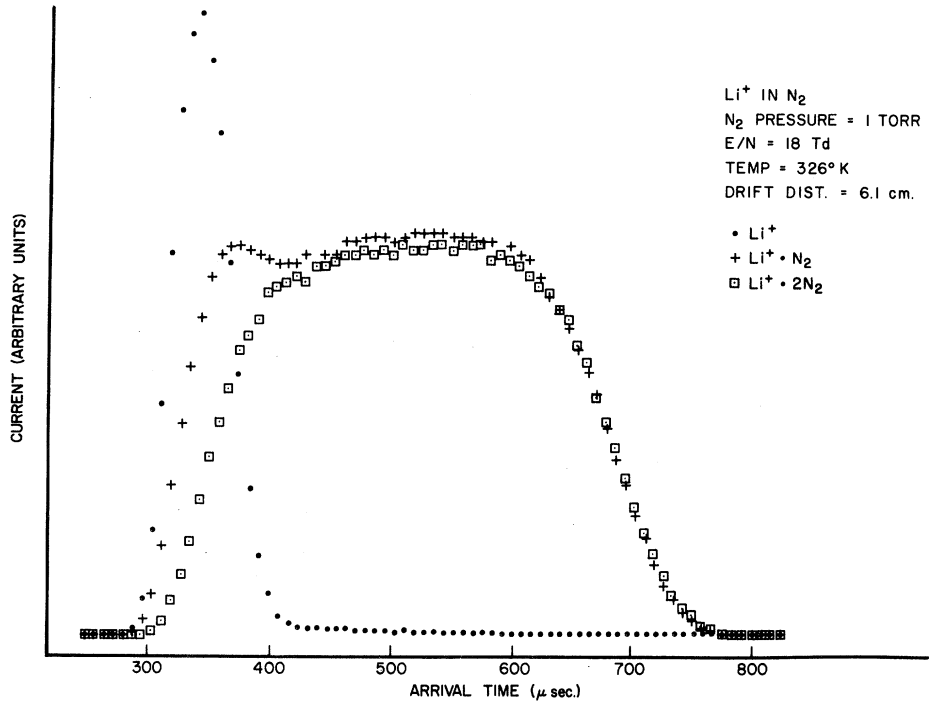

FIG. 2. Typical Li^+, $Li^+ \cdot N_2$, and $Li^+ \cdot 2N_2$ spectra superimposed.

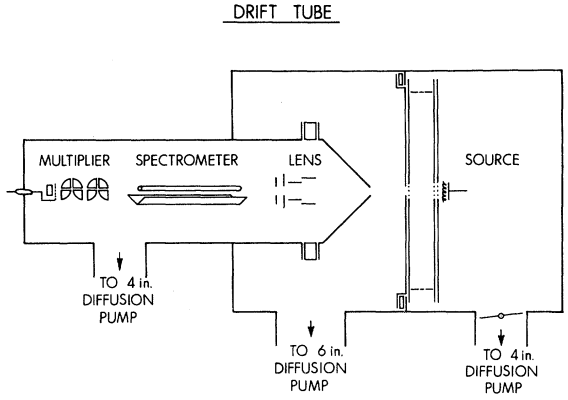

FIG. 3. Experimental configuration.

several hundred amu. The ions are detected by a 16 stage Ag-Mg multiplier, operated in a pulse-counting mode. These output pulses pass through a preamplifier, amplifier, and discriminator to both a counter and a 1024-channel time-of-flight analyzer.

The stainless-steel gas-feed line between the regulator and the drift tube has both a large reservoir tank and a U-tube trap. Enough gas for a week's operations was admitted to the feed line at one time; the trap was allowed to cleanse this gas sample at least overnight before the gas was used. This trap, maintained at a temperature of about -100 °C,[4] removed water and other impurities very effectively.

The gas pressure in the tube is measured by a Datametrics-Barocel bakable capacitance manometer. Its output is fed through a control circuit to a servo-driven variable-leak valve so that the gas pressure can be regulated at any fixed value to within 0.3 mTorr.

An iron-constantan thermocouple was used to monitor the gas temperature. It was placed just outside the drift region. The N_2-gas temperature was maintained at 318 ± 2 K for all work reported here, although other temperatures were occasionally used for tests. The effect that the hot source may have had on this work is discussed later.

Time-of-arrival spectra were reported at three pressures, typically 0.5, 1.0, and 1.5 Torr, for E/N values of 9, 12, 15, 18, 21, and 24 Td, where E is the uniform-electric-field strength in the drift region, N is the neutral number density, and $1\ \text{Td} = 10^{-17}\ \text{V cm}^2$.

III. THEORY

In this section the analysis of drifting, diffusing, and interconverting ion swarms,[5] previously only developed for two-ion species, is extended to three-ion species connected by a reaction scheme such as that defined by Eqs. (1) and (2).

The ion-swarm parameters and reaction rate coefficients will be labeled by the subscripts 1, 2, and 3 to indicate Li^+, $Li^+ \cdot N_2$, and $Li^+ \cdot 2N_2$, respectively. The drift velocities v_i $(i = 1, 2, 3)$ are related to the reduced mobilities K_{0i} by the relations

$$v_i = K_{0i} N_0 (E/N), \tag{4}$$

where $N_0 = 2.69 \times 10^{19}\ \text{cm}^{-3}$ (the gas number density at STP). The longitudinal diffusion coefficients D_{Li} are related to the reduced mobilities by the Einstein equation

$$N D_{Li} / N_0 K_{0i} = k T_i / q, \tag{5}$$

where q is the ion's charge, k is Boltzmann's constant, and T_i is the effective ion temperature. For low fields and slow reactions T_i is close to the neutral-gas temperature T. However, if the energy introduced into the system by the external field, or by reactions, is not negligible, it will contribute in part to the random motion of the ions, resulting in an elevated effective-ion temperature which may vary with the ion species. The transverse diffusion coefficients D_{Ti} are similarly related to the mobility, but may have separate effective temperatures, owing to the directional asymmetry introduced by the electric field. In the present application the results were insensitive to transverse diffusion so the approximation $D_{Ti} = D_{Li}$ was used for each species.

The reaction frequencies which represent the probability of converting one ion to another are given in terms of the rate coefficients and the neutral-gas number density as follows: For $Li^+ + 2N_2 \rightarrow Li^+ \cdot N_2 + N_2$

$$\alpha_{21} = N^2 k_{21}, \tag{6}$$

for $Li^+ \cdot N_2 + 2N_2 \rightarrow Li^+ \cdot 2N_2 + N_2$

$$\alpha_{32} = N^2 k_{32}, \tag{7}$$

for $Li^+ \cdot 2N_2 + N_2 \rightarrow Li^+ \cdot N_2 + 2N_2$

$$\alpha_{23} = N k_{23}, \tag{8}$$

and for $Li^+ \cdot N_2 + N_2 \rightarrow Li^+ + 2N_2$

$$\alpha_{12} = N k_{12}. \tag{9}$$

The total depletion frequencies for the three species are

$$\alpha_{01} = \alpha_{21}, \tag{10}$$

$$\alpha_{02} = \alpha_{12} + \alpha_{32}, \tag{11}$$

and

$$\alpha_{03} = \alpha_{23}, \tag{12}$$

assuming that reactions to other than the three species considered are negligible.

The ion-swarm number densities $n_i(\vec{r}, t)$ satisfy the coupled partial-differential equations[5]

$$\frac{\partial n_i}{\partial t} = \mathfrak{D}_i n_i + \sum_{j(\neq i)} \alpha_{ij} n_j , \tag{13}$$

where

$$\mathfrak{D}_i = D_{Ti}\left(\frac{\partial^2}{\partial x^2} + \frac{\partial^2}{\partial y^2}\right) + D_{Li}\frac{\partial^2}{\partial z^2} - v_i \frac{\partial}{\partial z} - \alpha_{0i} . \tag{14}$$

The boundary conditions are of minor consequence and will be discussed later. A general solution for such equations has been developed using a Green's-function sum-over-histories method.[5,6] If the ion source produces initial swarm densities $\beta_i(\vec{r})$ at $t=0$, then at time t and position $\vec{r}$ the ion-swarm densities are given by

$$n_i(\vec{r}, t) = \sum_j \int d^3r' \, G_{ij}(\vec{r} - \vec{r}', t)\beta_j(\vec{r}') , \tag{15}$$

where the Green's functions have the form

$$G_{ij}(\vec{r}, t) = \left(\prod_{q=1}^{p} \int_0^t d\tau_q\right) \delta\left(\sum_{q=1}^{p} \tau_q - t\right) F(\vec{r}, \vec{\tau}) Q_{ij}(\vec{\tau}) , \tag{16}$$

with $\vec{\tau} = (\tau_1, \tau_2, \ldots, \tau_p)$ for p distinct ion species in general. In the present case $p=3$. The function F is a Gaussian in configuration space,

$$F(\vec{r}, \vec{\tau}) = (\pi^3 r_T^4 r_L^2)^{-1/2} \times \exp\left[-(x^2+y^2)/r_T^2 - (z - r_D)^2/r_L^2 - \gamma_0\right] , \tag{17}$$

with a radial width r_T given by

$$r_T^2 = \sum_{q=1}^{p} 4 D_{Tq} \tau_q , \tag{18}$$

a longitudinal width r_L given by

$$r_L^2 = \sum_{q=1}^{p} 4 D_{Lq} \tau_q , \tag{19}$$

center position $(0, 0, r_D)$ where

$$r_D = \sum_{q=1}^{p} v_q \tau_q , \tag{20}$$

and spatial integral $e^{-\gamma_0}$ where

$$\gamma_0 = \sum_{q=1}^{p} \alpha_{0q} \tau_q . \tag{21}$$

The τ's actually represent the total time the ion spends as each species. The functions Q_{ij} involve a sum over all histories which start with species j and end with species i. A typical history might be written

$$i = q_k, q_{k-1}, \ldots, q_{s+1}, q_s \ldots, q_2, q_1 = j , \tag{22}$$

and should be read from right to left to obtain the chronological order. In general each species will be represented many times. Then Q_{ij} is a function of the total time in each species (τ_q for species q), the number of occurrences of each species in the history ($m_q + 1$ for species q), and the reaction frequencies from one species in the history to the next (e.g., α_{q_{s+1}, q_s}). The Q_{ij} may be formally written as

$$Q_{ij}(\vec{\tau}) = \sum_{\text{hist}} \left(\prod_{s=1}^{k-1} \alpha_{q_{s+1}, q_s}\right) \prod_{q=1}^{p} (\tau_q^{m_q}/m_q!) . \tag{23}$$

The special case in which a particular species is absent from the history should be treated using $p-1$ in place of p. However an equivalent procedure[5] is to use a δ function for that time variable, i.e.,

$$(\tau_q^{m_q}/m_q!)_{m_q=-1} = \delta(\tau_q) . \tag{24}$$

In general the evaluation of Q is cumbersome but readily simplifies in special cases. For the three-ion situation with no direct reaction-connecting species 1 and 3, the interior of the history must have the form

$$\cdots 2A2A \cdots 2A2 \cdots = \cdots 2(A2)^n \cdots \tag{25}$$

when the A's are either 1's or 3's. If n of the A's are 1's and l are 3's then the number of distinct histories of this type is

$$\binom{n+l}{n} = \frac{(n+l)!}{n!l!} . \tag{26}$$

Using this approach, all possible histories can be listed and summed. For present purposes the only source-produced ion is Li^+, i.e., species 1, and all histories with this initial ion are listed in Table I. From this table one finds

$$Q_{11} = \delta(\tau_2)\delta(\tau_3) + \delta(\tau_3)\alpha_{12}\alpha_{21}\tau_1 \sum_{n=0}^{\infty} \frac{(\alpha_{12}\alpha_{21}\tau_1\tau_2)^n}{n!(n+1)!} + \alpha_{12}\alpha_{21}\tau_1\alpha_{23}\alpha_{32}\tau_2 \sum_{n=0}^{\infty} \frac{(\alpha_{12}\alpha_{21}\tau_1\tau_2)^n}{n!(n+1)!} \sum_{l=0}^{\infty} \frac{(\alpha_{23}\alpha_{32}\tau_2\tau_3)^l}{l!(l+1)!}$$

$$= \delta(\tau_2)\delta(\tau_3) + \alpha_{12}\alpha_{21}\tau_1 (2/\eta) I_1(\eta)\phi , \tag{27}$$

TABLE I. Summation of ion histories for specified initial and final ions.

Hist ($A=1$ or 3)	m_1+1	m_2+1	m_3+1	mult	factor
$(1\rightarrow 1)$					
1	1	0	0	1	$\delta(\tau_2)\delta(\tau_3)$
$1(21)^{n+1}$	$n+2$	$n+1$	0	1	$\delta(\tau_3)(\alpha_{12}\alpha_{21})^{n+1}\tau_1^{n+1}\tau_2^n/(n+1)!n!$
$12(A2)^{n+l+1}1$	$n+2$	$n+l+2$	$l+1$	$\binom{n+l+1}{n}$	$\frac{(\alpha_{12}\alpha_{21})^{n+1}(\alpha_{23}\alpha_{32})^{l+1}\tau_1^{n+1}\tau_2^{n+l+1}\tau_3^l}{(n+1)!\,(n+l+1)!\,l!}$
$(1\rightarrow 2)$					
$(21)^{n+1}$	$n+1$	$n+1$	0	1	$\delta(\tau_3)\alpha_{21}(\alpha_{12}\alpha_{21})^n\tau_1^n\tau_2^n/(n!)^2$
$2(A2)^{n+l+1}1$	$n+1$	$n+l+2$	$l+1$	$\binom{n+l+1}{n}$	$\frac{\alpha_{21}(\alpha_{12}\alpha_{21})^n(\alpha_{23}\alpha_{32})^{l+1}\tau_1^n\tau_2^{n+l+1}\tau_3^l}{n!(n+l+1)!\,l!}$
$(1\rightarrow 3)$					
$32(A2)^{n+l}1$	$n+1$	$n+l+1$	$l+1$	$\binom{n+l}{n}$	$\frac{\alpha_{32}\alpha_{21}(\alpha_{12}\alpha_{21})^n(\alpha_{23}\alpha_{32})^l\tau_1^n\tau_2^{n+l}\tau_3^l}{n!(n+l)!\,l!}$

where

$$\phi = \delta(\tau_3) + \alpha_{23}\alpha_{32}\tau_2(2/\eta')I_1(\eta'), \tag{28}$$

with

$$\eta = (4\alpha_{12}\alpha_{21}\tau_1\tau_2)^{1/2} \tag{29}$$

and

$$\eta' = (4\alpha_{23}\alpha_{32}\tau_2\tau_3)^{1/2}; \tag{30}$$

also

$$Q_{21} = \delta(\tau_3)\alpha_{21}\sum_{n=0}^{\infty}\frac{(\alpha_{12}\alpha_{21}\tau_1\tau_2)^n}{(n!)^2} + \alpha_{21}\sum_{n=0}^{\infty}\frac{(\alpha_{12}\alpha_{21}\tau_1\tau_2)^n}{(n!)^2}\,\alpha_{23}\alpha_{32}\tau_2\sum_{l=0}^{\infty}\frac{(\alpha_{23}\alpha_{32}\tau_2\tau_3)^l}{l!(l+1)!}$$
$$= \alpha_{21}I_0(\eta)\phi \tag{31}$$

and

$$Q_{31} = \alpha_{32}\alpha_{21}\sum_{n=0}^{\infty}\frac{(\alpha_{12}\alpha_{21}\tau_1\tau_2)^n}{(n!)^2}\sum_{l=0}^{\infty}\frac{(\alpha_{23}\alpha_{32}\tau_2\tau_3)^l}{(l!)^2}$$
$$= \alpha_{32}\alpha_{21}I_0(\eta)I_0(\eta'). \tag{32}$$

I_0 and I_1 are the modified Bessel functions of the first kind and order 0 and 1, respectively.

For the three-ion case the δ function in Eq. (16) will reduce the expression for the Green's function to a double integration,

$$\prod_{q=1}^{3}\int_0^t d\tau_q\,\delta\left(\sum_{q=1}^{3}\tau_q - t\right) = \int_0^t dt_1\int_0^{t_1}dt_2\Big|_{\vec{\tau}=(t-t_1,\,t_1-t_2,\,t_2)}, \tag{33}$$

and this will further reduce to a single integration or no integration for those terms in Q which include δ functions.

The character of the source is not fully known but fortunately the process of diffusion makes the observed spectra insensitive to the details of the initial ion distribution. The distribution which provides the greatest simplification in the analysis while allowing enough variation to test sensitivity to the behavior of the source is a Gaussian,

$$\beta(\vec{r}) = C_1(\pi r_0^4 z_0^2)^{-1/2}e^{-(x^2+y^2)/r_0^2 - z^2/z_0^2}, \tag{34}$$

with radial width r_0 and longitudinal width z_0. For this source distribution

$$n_i(\vec{r},t) = C_1 G_{i1}(\vec{r},t)\Big|_{\substack{r_T^2\rightarrow r_T^2+r_0^2\\ r_L^2\rightarrow r_L^2+z_0^2}}; \tag{35}$$

i.e., apart from a constant, C_1, which specifies the number of ions leaving the source, the expressions for n are the same as for G if the diffusion widths are redefined.

The resulting solutions are valid provided that the ion swarms are developing in an unbounded region. As far as the radial diffusion is concerned, r_T is always small compared with the radius of the drift tube so the effect of the cylindrical walls can be ignored. On the other hand the ions are produced by a source in one end plate and sampled through an aperture in the other end plate so that the longitudinal boundary conditions cannot be disposed of so lightly. Imposing the conditions that the number densities vanish at the source end plate ($z=0$) for all positive times and vanish at the detector end plate ($z=l$) for all times can be easily approximated if it is assumed that the three ions

are at the same effective temperature, so that $4D_{L1}/v_1 = 4D_{L2}/v_2 = 4D_{L3}/v_3 = \rho$, and that $\rho \ll l$. From the character of the differential equation (13) it is apparent that $\partial n_i/\partial z$ are also solutions and, by inspection, one finds that

$$n_i' = n_i - \tfrac{1}{2}\rho \frac{\partial n_i}{\partial z} \tag{36}$$

satisfy the boundary conditions at $z = 0$ and have the same source strength. The boundary conditions at $z = l$ are satisfied by adding solutions appropriate to an image source at $z = 2l$, i.e.,

$$n_i'' = n_i'(z) + n_i'(z - 2l)e^{l/\rho}. \tag{37}$$

It should be noted that this violates the boundary conditions at $z = 0$ but only by an amount of order $(\rho/l)^2$ which, for all practical purposes, is negligible.

The observed time-of-arrival spectra are proportional to the ion currents through the small on-axis aperture (area A) in the end plate. Theoretically they are given by

$$W_i(t) = \epsilon_i A\left(v_i n_i'' - D_{Li}\frac{\partial n_i''}{\partial z}\right)_{\vec{r}=l\hat{z}}$$
$$= \epsilon_i A v_i \int_0^t dt_1 \int_0^{t_1} dt_2\, (l/r_D)^2 F_0(l, \vec{\tau}) Q_{i1}(\vec{\tau}) C_1, \tag{38}$$

where $\vec{\tau} = (t - t_1, t_1 - t_2, t_2)$, ϵ_i are the detection efficiencies for the three ions, and terms of order $(\rho/l)^2$ have been ignored. The function F reduces to F_0, given by

$$F_0(l, \vec{\tau}) = (\pi^3 r_T^4 r_L^2)^{-1/2} e^{-(l-r_D)^2/r_L^2 - \gamma_0}, \tag{39}$$

where now

$$r_T^2 = 4D_{T1}\tau_1 + 4D_{T2}\tau_2 + 4D_{T3}\tau_3 + r_0^2, \tag{40}$$

$$r_L^2 = 4D_{L1}\tau_1 + 4D_{L2}\tau_2 + 4D_{L3}\tau_3 + z_0^2, \tag{41}$$

$$r_D = v_1\tau_1 + v_2\tau_2 + v_3\tau_3, \tag{42}$$

and

$$\gamma_0 = \alpha_{01}\tau_1 + \alpha_{02}\tau_2 + \alpha_{03}\tau_3. \tag{43}$$

The Q's are those given by Eqs. (27)–(32) and the term $(l/r_D)^2$ arises from the boundary conditions. Since the function F_0 is only large for $r_D \approx l$, the boundary-condition term is effectively unity and can be omitted without changing the results. Once the δ functions in Q have been allowed for, the other integrations may be carried out numerically. This procedure is facilitated by the dominance of the function F_0 in the behavior of the integrand since values of $\vec{\tau}$ for which $(l - r_D)^2 \gg r_L^2$ can be discounted.

IV. COMPARISON OF THEORY AND EXPERIMENT

Three minor details complicate the comparison between the theoretical and experimental spectra. First, the source strength C_1 and detection efficiencies ϵ_i are not known. Since these do not affect the shape they are chosen to normalize the theoretical spectrum so that its area matches that of the experimental spectrum. Second, the channel width Δt of the detector is not negligibly small. To take account of this the theoretical curve is interpolated and at the same time diffused over two channels to allow for the finite time width of the source and detector. The formula used is

$$\overline{W}_i((n+\lambda)\Delta t) = \tfrac{1}{4}\{(1-\lambda)^2 W_i((n-1)\Delta t) + (2-\lambda^2)W_i(n\Delta t)$$
$$+ [2 - (1-\lambda)^2]\, W_i((n+1)\Delta t)$$
$$+ \lambda^2 W_i((n+2)\Delta t)\}, \tag{44}$$

where $0 \leq \lambda < 1$. Since this allows for initial longitudinal broadening in the source gate, $z_0 = 0$ yields satisfactory results. Third, the time delay t_0 in recording each event is not known exactly so that the time appropriate to channel m is $(m + \frac{1}{2})\Delta t + t_0$. In comparing the experimental and theoretical spectra t_0 is varied until the best fit is obtained. This is accomplished by displacing the experimental spectrum an exact number of channels and then interpolating the theoretical spectrum by using an appropriate value of λ in Eq. (44). This avoids smoothing the experimental data, which would systematically influence the goodness-of-fit test. In this regard it should be noted that both $\overline{W}$ and its first time derivative are continuous.

The effects of radial diffusion and the finite source size only enter through the term r_T^2 in Eq. (39). If the value of ρ $(= 4D_T/v)$ is the same for all three ions then

$$r_T^2 = \rho r_D + r_0^2 \approx \rho l + r_0^2 \tag{45}$$

when F_0 is large, so that the first-order contribution is just a constant. Further, the value of this constant is of no consequence since it is absorbed by the normalization procedure. Indeed the normalized theoretical spectra are found to be quite insensitive to the value of r_0. In practice $r_0 = 1$ cm was used to approximate the physical size of the source aperture.

With the techniques given above, Eq. (38) was used to generate the theoretical spectra, which were interpolated according to Eq. (44) for comparison with the individual points comprising the experimental spectra. If one substitutes Eqs. (4)–(12), (27)–(32), and (39)–(43) for the various factors in Eq. (38), it can be shown that the theoretical spectra are determined only by the mea-

sured swarm parameters K_{0i}, T_i, and k_{ij}, and by the fixed parameters E/N, N (pressure), and the drift distance.

Experimental spectra for low E/N and high pressure are shown in Figs. 4–6 for each ion species and spectra for high E/N and low pressure are shown in Figs. 7–9. Certain general features are apparent. For a given E/N and pressure the Li^+ drift velocity is easily determined by the Li^+ peak position with an allowance for the detector delay time obtained from measurements with a very short drift distance. The average drift velocity of the $Li^+ \cdot N_2$ and $Li^+ \cdot 2N_2$ ions is determined by the width of the $Li^+ \cdot N_2$ (or $Li^+ \cdot 2N_2$) spectrum once the Li^+ drift velocity is known. Since the $Li^+ \cdot N_2 + 2N_2 \rightarrow Li^+ \cdot 2N_2 + N_2$ reaction is three body and the reverse reaction is two body the relative population of the two species varies considerably with variation of pressure. The observation that the average drift velocity varies very little with pressure implies that the individual $Li^+ \cdot N_2$ and $Li^+ \cdot 2N_2$ drift velocities are close to each other. The effective ion temperature, which determines the diffusion coefficients, only influences the Li^+ peak width and the steepness of the edges of the $Li^+ \cdot N_2$ and $Li^+ \cdot 2N_2$ spectra. The similarity of the $Li^+ \cdot N_2$ and $Li^+ \cdot 2N_2$ spectra indicates that the reactions between these species are fast, i.e., k_{32} and k_{23} are large. The accuracy of the estimates of k_{32} and k_{23} depends on the differences between the $Li^+ \cdot N_2$ and the $Li^+ \cdot 2N_2$ spectra; the most pronounced case is shown in Figs. 8 and 9. The well-defined slope of the central portion of the $Li^+ \cdot N_2$ spectrum, as in Fig. 5, provides a good estimate of k_{21}. The smallness of the extended tail or "foot" in the Li^+ spectrum, relative to the peak implies that the back reaction to Li^+ is slow, i.e., k_{12} is small.

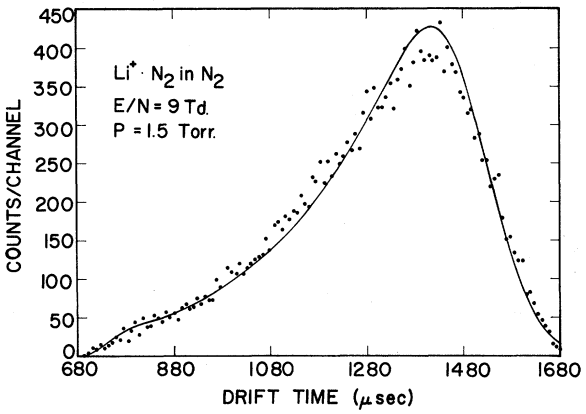

FIG. 5. $Li^+ \cdot N_2$ spectrum at an E/N of 9 Td and a pressure of 1.5 Torr. The points denote the experimental spectrum and the line is the theoretical result which gives the best fit at all three pressures.

These various features may be used to obtain initial estimates of the kinetic parameters, which are then refined by detailed comparison of the theoretical and experimental spectra.

Refined fits were made using independent sets of kinetic parameters (K_{0i}, T_i, k_{ij}) at each value of E/N. In each case this involved spectra from each of the three ion species at three distinct pressures. For $E/N = 9$, 15, 18, 21 and 24 Td the pressures were 0.5, 1.0, and 1.5 Torr and at $E/N = 12$ Td the pressures were 0.6, 1.0, and 1.4 Torr. The reduced mobilities appeared to be independent of E/N and their values were 3.87 $cm^2/V\,sec$ for Li^+

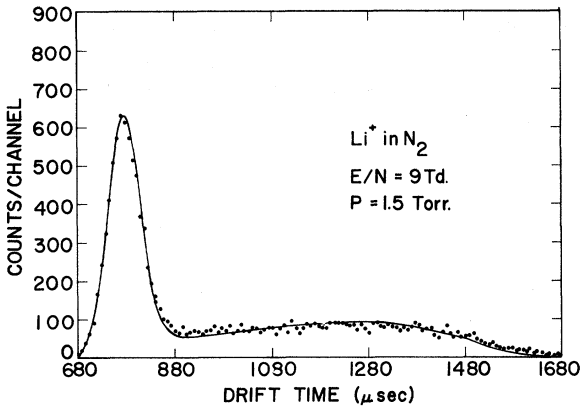

FIG. 4. Li^+ spectrum at an E/N of 9 Td and a pressure of 1.5 Torr. The points denote the experimental spectrum and the line is the theoretical results which gives the best fit at all three pressures.

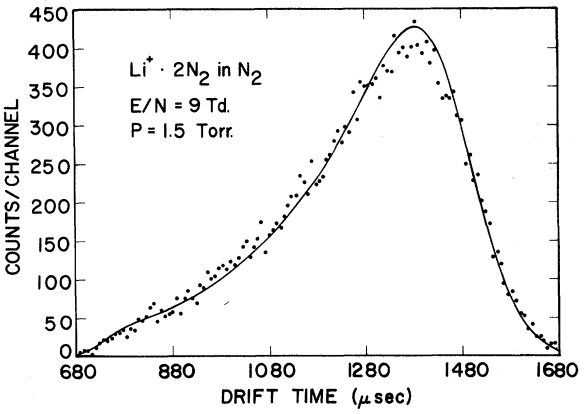

FIG. 6. $Li^+ \cdot 2N_2$ spectrum at an E/N of 9 Td and a pressure of 1.5 Torr. The points denote the experimental spectrum and the line is the theoretical result which gives the best fit at all three pressures.

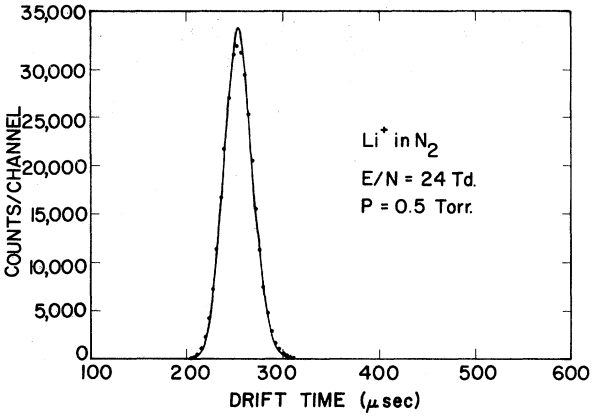

FIG. 7. Li^+ spectrum at an E/N of 24 Td and a pressure of 0.5 Torr. The points denote the experimental spectrum and the line is the theoretical result which gives the best fit at all three pressures.

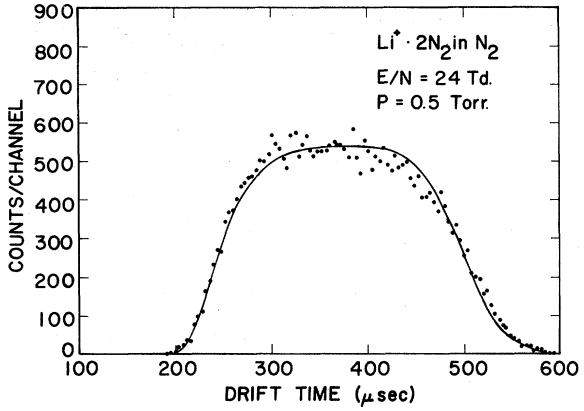

FIG. 9. $Li^+ \cdot 2N_2$ spectrum at an E/N of 24 Td and a pressure of 0.5 Torr. The points denote the experimental spectrum and the line is the theoretical result which gives the best fit at all three pressures.

in N_2, 2.04 cm^2/V sec for $Li^+ \cdot N_2$ in N_2, and 1.96 cm^2/V sec for $Li^+ \cdot 2N_2$ in N_2, all at a neutral-gas temperature of 318 K.

The effective ion temperature of the Li^+ ion, T_1, was always close to that of the neutral gas, T. The best-fit value of T_1/T ranged from 1.0 at low E/N to 1.1 at high E/N, but the departure from unity was not statistically significant. For the $Li^+ \cdot N_2$ and $Li^+ \cdot 2N_2$ ions, however, T_i/T ranged from 1.5 at low E/N and low pressure to 2.4 at high E/N and high pressure. Owing to the fast forward-backward reaction between the $Li^+ \cdot N_2$ and $Li^+ \cdot 2N_2$ ions it is not possible to distinguish different temperatures for the two ions so, for present purposes, it is assumed that $T_2 = T_3$ in each case. Values of T_2/T ($= T_3/T$) are given in Table II for the various E/N and pressure values.

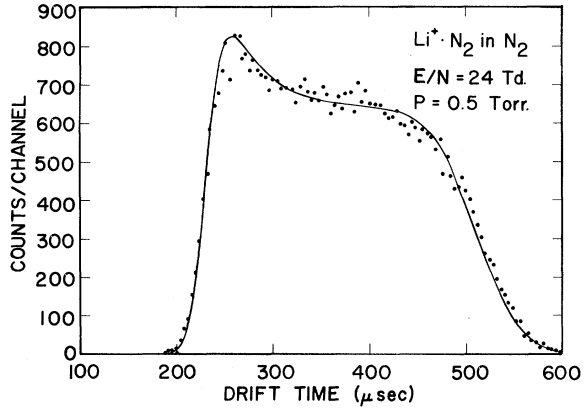

FIG. 8. $Li^+ \cdot N_2$ spectrum at an E/N of 24 Td and a pressure of 0.5 Torr. The points denote the experimental spectrum and the line is the theoretical result which gives the best fit at all three pressures.

As mentioned previously the determination of the reaction rate coefficients is made somewhat uncertain by the fast forward-backward reactions between $Li^+ \cdot N_2$ and $Li^+ \cdot 2N_2$ ions. In the absence of any independent data adequate fits could be obtained with values of k_{32} ranging from 1.6 to $3.0(\times 10^{-29})$ cm^6/sec. Using a median value of 2.2×10^{-29} cm^6/sec for the $Li^+ \cdot N_2 + 2N_2 \rightarrow Li^+ \cdot 2N_2 + N_2$ reaction rate coefficient yields the following results. The $Li^+ + 2N_2 \rightarrow Li^+ \cdot N_2 + N_2$ reaction rate coefficient k_{21} decreases from 2.0×10^{-30} cm^6/sec at $E/N = 9$ Td to 1.7×10^{-30} cm^6/sec at $E/N = 24$ Td, the $Li^+ \cdot N_2 + N_2 \rightarrow Li^+ + 2N_2$ reaction rate coefficient k_{12} increases from 0.7×10^{-14} cm^3/sec at $E/N = 9$ Td to 1.6×10^{-14} cm^3/sec at $E/N = 24$ Td, and the $Li^+ \cdot 2N_2 + N_2 \rightarrow Li^+ \cdot N_2 + 2N_2$ rate coefficient k_{23} increases from 4.8×10^{-13} cm^3/sec at $E/N = 9$ Td to 6.0×10^{-13} cm^3/sec at $E/N = 24$ Td. Reaction rate coefficients for each value of E/N are listed in Table III. Much of the uncertainty in the reaction-rate-coefficient determination could be eliminated if the relative detection efficiency for $Li^+ \cdot N_2$ and $Li^+ \cdot 2N_2$ ions were known since then the

TABLE II. Estimates of the ratio of the cluster ions's effective temperature to the neutral-gas temperature.

E/N (Td) \ Press (Torr)	0.5	1.0	1.5
9	1.5	1.5	1.5
12	1.6 [a]	1.7	1.8 [b]
15	1.7	1.8	1.9
18	1.7	2.0	2.1
21	1.7	2.2	2.4
24	1.8	2.2	2.4

[a] 0.6 Torr. [b] 1.4 Torr.

TABLE III. Estimates of the reaction rates k_{21} ($Li^+ + 2N_2 \rightarrow Li^+ \cdot N_2 + N_2$), k_{12} ($Li^+ \cdot N_2 + N_2 \rightarrow Li^+ + 2N_2$), k_{32} ($Li^+ \cdot N_2 + 2N_2 \rightarrow Li^+ \cdot 2N_2 + N_2$), and k_{23} ($Li^+ \cdot 2N_2 + N_2 \rightarrow Li^+ \cdot N_2 + 2N_2$).

E/N	k_{21} (10^{-30} $cm^6\,sec^{-1}$)	k_{12} (10^{-14} $cm^3\,sec^{-1}$)	k_{32} (10^{-29} $cm^6\,sec^{-1}$)	k_{23} (10^{-13} $cm^3\,sec^{-1}$)
9	2.0	0.7	2.2	4.8
12	1.9	0.9	2.2	5.0
15	1.9	1.3	2.2	5.1
18	1.8	1.2	2.2	5.4
21	1.8	1.7	2.2	5.8
24	1.7	1.6	2.2	6.0

forward and backward reaction rate coefficients could be determined and this would provide the additional piece of information needed in the analysis.

The fact that the $Li^+ \cdot N_2$ and $Li^+ \cdot 2N_2$ ion swarms are in equilibrium over most of the spectrum also makes it impossible to determine whether the Li^+ ions in the tail of the Li^+ spectra are produced by the reaction

$$Li^+ \cdot N_2 + N_2 \rightarrow Li^+ + 2N_2 \tag{46}$$

or by

$$Li^+ \cdot 2N_2 + N_2 \rightarrow Li^+ + 3N_2. \tag{47}$$

The region in which the $Li^+ \cdot N_2$ and $Li^+ \cdot 2N_2$ spectra differ occurs at the same time as the peak of unreacted Li^+ ions. Also the Li^+ spectrum tail is too small at low pressures to permit a test based on the pressure variation of the relative $Li^+ \cdot N_2$ and $Li^+ \cdot 2N_2$ population. The results quoted here for the values of k_{12} assume that reaction (47) does not occur.

Use of the tabulated values of K_{0i}, T_i, and k_{ij} yields theoretical spectra, at all E/N values and all pressures, which are in good agreement with the experimental time-of-arrival spectra except in one detail. The regions of the experimental time-of-arrival spectra corresponding to ions which have spent very little time as Li^+ appear to be too low. This effect is evidence of a reduction in the $Li^+ + 2N_2 \rightarrow Li^+ \cdot N_2 + N_2$ reaction frequency close to the source and is probably due to local heating of the gas in that region. This would reduce the three-body reaction rate coefficient k_{21}, and also the neutral-gas number density N, both of which lead to a lowering of the reaction frequency α_{21}. An over-simplified model with a reduction factor $c(1 - v_1\tau_1/d)$ for $\tau_1 < d/v_1$ was included with F in Eq. (38) to test this possibility. The desired effect was reproduced with $c = 0.3$ and $d = 2$ cm. The factor of $c = 0.3$ could be accounted for by (a) a decrease in k_{21} of 30% (if T were held constant), *or* (b) an increase of 50 °C in T (if k_{21} were held constant) *or* (c) some combination of lesser changes of these two parameters. Setting $d = 2$ cm causes the effect to diminish to zero at 2 cm down the tube from the source.

V. ERROR ANALYSIS

Uncertainties in the deduced values of the kinetic coefficients arise from three sources. First, there are inaccuracies in the measurement of the experimental parameters: pressure, electric field, temperature, distance, and time. These have been discussed previously and are at most a few percent. They are negligible when compared with other errors except for one parameter, the mobility of Li^+ in N_2, where they contribute the predominant error of 2.5%.

Second, there are statistical errors associated with the experimental data where the counts per channel for the cluster ions has a maximum ranging from about 300 to 3000, depending on pressure and E/N. The statistical errors in the kinetic coefficients are best determined by isolating the portions of the experimental spectra which are most sensitive to the coefficient in question. For the drift velocities and diffusion coefficients of the cluster ions, only the edges of the cluster-ion spectra are of consequence, while the reaction rate coefficients are more sensitive to the interior parts of these spectra.

The statistical error in estimating the position and spread of the sharp rise and fall at the edges of the spectra are typically between 1 and 2 channel widths, making a contribution to the error in the reduced-mobility determination for the cluster ions of less than 5%, and to the effective ion temperature of about 12%.

The estimate of k_{21} in cases where the $Li^+ \cdot N_2$ and $Li^+ \cdot 2N_2$ spectra are similar, as in Figs. 5 and 6, is insensitive to the values of the other reaction rate coefficients. The statistical error in the measurement of k_{21} varied from 7% at high E/N to 15% at low E/N, based primarily on the high-pressure data.

As mentioned above, k_{32} and k_{23} are large enough to establish equilibrium between the two cluster ion species after a very short time so that at most a few channels in the time-of-arrival spectra exhibit a difference between the $Li^+ \cdot N_2$ and $Li^+ \cdot 2N_2$ relative counting rates. In the most advantageous case, as shown by Figs. 8 and 9, the nonequilibrium region occupies about 25 channels in the $Li^+ \cdot N_2$ spectrum and the counts per channel drops from about 825 to 650. This gives an estimated error of 55% in the value of k_{32}, which depends directly on the slope. The magnitude of the difference between the $Li^+ \cdot N_2$ and $Li^+ \cdot 2N_2$ spectra is found, empirically, to vary with k_{23}^2/k_{32}, so that the major error in the estimate of k_{23} arises from the error in k_{32}. Thus the value of k_{23} has an estimated error of 30%.

The estimate of k_{12} is based on the area in the foot of the Li^+ spectrum, for which the statistical error is 1% or less, but also depends on $k_{21}k_{23}/k_{32}$ if the assumptions in Sec. I are valid. If k_{23}/k_{32} were known, the error in the estimate of k_{12} would be about 7 to 15%. However, in view of the theoretical and experimental uncertainites, a 55% error is the best that can be claimed with the present data.

Third, there are errors associated with the apparent heating of the gas close to the source. If the entire effect were associated with a change in the gas temperature, and thus a change in the gas number density, then $c = 0.3$ and $d = 2$ cm implies an average 2% change in the gas number density throughout the drift region.

Combining these three sources of error leads to the following estimates of the standard deviations for each determination: 3.4% for the reduced mobility of Li^+ in N_2, 6% for the reduced mobility of the cluster ions, 15% for the effective ion temperatures, 9 to 17% for k_{21}, 55% for k_{12} and k_{32}, and 30% for k_{23}.

VI. COMPARISON WITH OTHER MEASUREMENTS

We know of one other measurement of the clustering of N_2 to Li^+. Spears and Ferguson[7] used a flowing afterglow facility to study the clustering of several gases to Li^+. They deduced a rate constant of 8.0×10^{-31} cm^6/sec for the reaction

$$Li^+ + N_2 + He \rightarrow Li^+ \cdot N_2 + He$$

from the depletion of Li^+. That compares very well with our value of 2.0×10^{-30} cm^6/sec. One would expect our value to be larger because N_2 is a more effective third body than He.

There are at least two other measurements of the mobility of Li^+ in N_2. Tyndall[8] obtained a value for the zero-field reduced mobility of Li^+ in N_2 at 291 K of 3.95 cm^2/V sec. Takata[9] used a drift-tube mass spectrometer to study the mobility for Li^+ in H_2, N_2, and their mixtures. He found that the zero-field reduced mobility for Li^+ in N_2 at 299 to 311 K is 4.1 cm^2/V sec. Both of these measurements are in good agreement with our value at 318 K of 3.87 ± 0.13 cm^2/V sec.

ACKNOWLEDGMENTS

We wish to thank our many colleagues at BRL and Georgia Tech for their inspiration and critical comments in the course of this work. One of us (I. R. G.) was employed under the Laboratory Research Cooperative Program, administered through the Army Research Office.

---

*Permanent address: School of Physics, Georgia Institute of Technology, Atlanta, Ga. 30332. Research supported in part by the Atmospheric Sciences Section, National Science Foundation.

[1]G. E. Keller, R. A. Beyer, and L. M. Colonna-Romano, Phys. Rev. A 8, 1446 (1973).

[2]G. E. Keller and L. M. Romano, Bull. Am. Phys. Soc. 17, 392 (1972).

[3]We wish to thank Professor E. W. McDaniel for his gift of this material.

[4]L. J. Puckett, M. W. Teague, and D. G. McCoy, Rev. Sci. Instrum. 42, 580 (1971).

[5]I. R. Gatland, Case Studies At. Phys. 4, 369 (1974).

[6]In Ref. 5 the assumption is made (p. 378) that the reactive collision rate is small with respect to the elastic collision rate so that it can be neglected in the momentum equation. If this were not the case, we would not observe time-of-arrival spectra which were not in equilibrium under the conditions of this experiment. The effect of reactive collisions on the momentum equation is discussed by T. V. Vorburger, S. B. Woo, and J. H. Whealton, J. Appl. Phys. 44, 2571 (1973).

[7]K. G. Spears and E. E. Ferguson, J. Chem. Phys. 59, 4174 (1973).

[8]A. M. Tyndall, *The Mobility of Positive Ions in Gases* (Cambridge U. P., Cambridge, England, 1938), p. 92.

[9]N. Takata, Phys. Rev. A 10, 2336 (1974).